# Compact Zigzag Vibration Isolator Based on Additive Manufacturing

JIA Meng, WANG Tingwei, DAI Ning\*

College of Mechanical and Electrical Engineering, Nanjing University of Aeronautics and Astronautics, Nanjing 210016, P. R. China

(Received 12 June 2025; revised 29 July 2025; accepted 25 September 2025)

Abstract: Devices on aircraft are subjected to complex environmental excitations that pose risks to their operational safety. Passive vibration isolation techniques are extensively employed due to their advantage of not requiring additional energy sources. This paper introduces a novel metallic vibration isolator based on zigzag structures. The proposed isolator features a compact design and can be manufactured using additive manufacturing techniques, allowing for the integration of structural and functional elements. Firstly, the vibration response of the single-degree-of-freedom (SDOF) system is analyzed. To achieve effective vibration reduction, it is crucial for the isolator's stiffness to be sufficiently low. Secondly, to obtain a structure with high compliance, the traversal algorithm and the finite element method (FEM) are applied. The results confirm that the zigzag structure is a reliable high-compliance configuration. Thirdly, the parametric geometric model of the zigzag structure is developed and its stiffness is calculated. Quasi-static compression experiments validate the accuracy of the calculations. Finally, a specific engineering example is considered, where a zigzag vibration isolator is designed and fabricated. Vibration experiments demonstrate that the zigzag isolator effectively reduces both the stiffness and the fundamental frequency of the vibration system, achieving a vibration isolation efficiency exceeding 60%.

**Key words:** vibration isolation; passive isolators; additive manufacturing; zigzag structures; metallic vibration isolator **CLC number:** TH122 **Document code:** A **Article ID:** 1005-1120(2025)S-0121-10

#### 0 Introduction

Devices on aircraft face complex environmental excitations. Mechanical vibrations caused by airflow disturbances, pose adjustments, and rotor rotation are almost always present, affecting the operational reliability of electronic equipment and the lifespan of components. In severe cases, this can even lead to mechanical failure and safety incidents<sup>[1]</sup>. Therefore, it is crucial to design vibration and shock isolation for important equipment<sup>[2-3]</sup>.

An isolation device installed between the foundation and the protected equipment to reduce vibration excitation is known as an isolator. Isolators can be categorized into active and passive types<sup>[4-5]</sup>. A comprehensive review of passive vibration isolation

measures is provided in Ref. [6]. Due to their lack of need for additional energy sources, passive isolators are widely used in vibration scenarios. Depending on the material, commonly used isolators can be divided into metal and non-metal types. Due to limitations in environmental temperature and durability, metal isolators are more suitable for use on aircraft. Common metal isolators include helical springs<sup>[7]</sup>, leaf springs<sup>[8-9]</sup>, metal mesh<sup>[10]</sup>, metal rubber<sup>[11-12]</sup>, and wire ropes<sup>[13-14]</sup>. Helical springs are the most basic vibration isolation components but typically require significant installation space.

In recent years, with the development of additive manufacturing technology, complex structures such as lattice structures<sup>[15-16]</sup>, honeycomb structures<sup>[17-19]</sup>, and triply periodic minimal surfaces<sup>[20-22]</sup>

<sup>\*</sup>Corresponding author, E-mail address: dai\_ning@nuaa.edu.cn.

have been successfully manufactured. These structures have achieved wide applications in lightweight design, heat dissipation, and cushioning, and advancements in manufacturing processes have driven the emergence of new configurations. Chen et al. [23] replaced the straight edges of classic honeycombs with sinusoidal curves to create a series of novel honeycomb configurations. Ref. [24] significantly improved the energy absorption capability of cushioning structures by arranging smaller circular honeycombs around a larger circular honeycomb. Additive manufacturing not only allows for the processing of complex structures but also simplifies the assembly relationships between simplified structures, thereby reducing the number of parts and simplifying the manufacturing process. Xu et al. [25] used additive manufacturing to create a fabric with adjustable stiffness, simplifying the manufacturing process through one-step molding, resulting in a bending modulus increase of over 60 times. Due to this excellent performance, integrated structural-functional parts are increasingly favored by researchers, and their application is crucial for reducing equipment weight and enhancing aircraft performance.

This paper addresses the vibration isolation needs for aircraft equipment and proposes a novel isolator configuration based on metal additive manufacturing technology. To achieve this, the response characteristics of the vibration system are first analyzed. To find a suitable configuration, a depth-first search (DFS) and backtracking algorithm, combined with finite element analysis, demonstrated that the L-shaped beam is the most flexible configuration. Based on this, a parametric geometric model of the zigzag isolator is proposed. The stiffness of the isolator in the elastic phase is calculated and verified. Finally, the vibration reduction performance of the proposed zigzag isolator is validated for a specific engineering application.

#### 1 Theoretical Analysis

#### 1.1 Vbration response characteristics analysis

The mechanical model of the single-degree-of-freedom (SDOF) vibration system with base excita-

tion is shown in Fig. 1, where m is the mass of the protected object, k the stiffness of the isolator, c the damping,  $z_0(t)$  the displacement of the base, and  $z_1(t)$  the displacement of the protected object.

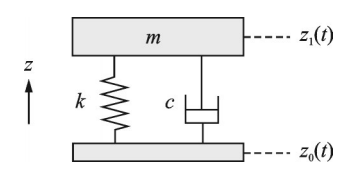


Fig.1 SDOF vibration system model with base excitation

The displacement of the protected object relative to the base can be denoted as  $\delta = z_1 - z_0$ . The motion equation of the system can be written as

$$\ddot{\delta} + 2\xi \omega_{n} \dot{\delta} + \omega_{n}^{2} \delta = -\ddot{z}_{0} \tag{1}$$

where  $\omega_{\rm n}=\sqrt{k/m}$  is the system's natural frequency of the system, and  $\xi=c/(2m\omega_{\rm n})$  the system's damping ratio. In engineering applications, vibration isolation devices generally satisfy  $0<\xi<1$ . When the base excitation is a harmonic vibration, let  $z_0=A_0\sin(\omega_0t)$ , where  $A_0$  is the displacement amplitude and  $\omega_0=2\pi f$ , with f being the excitation frequency. Then, it can be obtained that

$$\ddot{z}_0 = -A_0 \omega_0^2 \sin(\omega_0 t) \tag{2}$$

Let  $A = -A_0 \omega_0^2$  and  $\omega = \omega_0$ . Given the initial conditions  $\delta(0) = 0$  and  $\dot{\delta}(0) = 0$ , the solution can be obtained as

$$\delta = e^{-\xi \omega_{a} t} (C_{1} \cos(\omega_{d} t) + C_{2} \sin(\omega_{d} t)) + R_{1} \cos(\omega_{0} t) + R_{2} \sin(\omega_{0} t)$$
(3)

where  $R_1 = \frac{2\xi \omega_n \omega_0 A}{\left(\omega_n^2 - \omega_0^2\right)^2 + \left(2\xi \omega_n \omega_0\right)^2}, \quad R_2 = \frac{2\xi \omega_n \omega_0 A}{\left(\omega_n^2 - \omega_0^2\right)^2 + \left(2\xi \omega_n \omega_0\right)^2}$ 

$$\frac{-(\omega_{n}^{2}-\omega_{0}^{2})A}{(\omega_{n}^{2}-\omega_{0}^{2})^{2}+(2\xi\omega_{n}\omega_{0})^{2}}, \qquad C_{1}=-R_{1}, \qquad C_{2}=$$

$$rac{-oldsymbol{arphi}_{ ext{n}}R_{1}-R_{2}oldsymbol{\omega}_{0}}{oldsymbol{\omega}_{ ext{d}}}$$
 ,  $oldsymbol{\omega}_{ ext{d}}=\sqrt{1-oldsymbol{\xi}^{2}}\,oldsymbol{\omega}_{ ext{n}}$  .  $ar{\delta}=\mathrm{e}^{-oldsymbol{\xi}\omega_{ ext{n}}t}$  .

 $(C_1 \cos(\omega_d t) + C_2 \sin(\omega_d t))$  represents the damped vibration in the presence of damping. Typically, we consider the steady-state response of the system after it has stabilized, which is

$$\delta^* = R_1 \cos(\omega_0 t) + R_2 \sin(\omega_0 t) \tag{4}$$

Then, it can be obtained

$$z_1 = \delta^* + z_0 = R_1 \cos(\omega_0 t) + R_2 \sin(\omega_0 t) + A_0 \sin(\omega_0 t)$$
(5)

The steady-state response of the SDOF system

under harmonic excitation can be determined, as shown in Fig.2. The horizontal axis  $\Omega$  represents the ratio of the excitation frequency to the system's natural frequency, while the vertical axis  $z_1/z_0$  represents the ratio of the response amplitude to the maximum displacement of the excitation. It shows that when the excitation frequency is greater than  $\sqrt{2}$ times the natural frequency, the peak displacement response is less than the peak excitation. Thus, for passive vibration isolation, a lower system natural frequency results in a wider vibration isolation bandwidth. This implies that the stiffness of the isolator should be kept as low as possible. In the field of vibration isolation, a type of device known as a quasizero stiffness isolator<sup>[26-27]</sup> is designed to achieve lowfrequency isolation. However, quasi-zero stiffness isolators have poor lateral stiffness and typically require additional guiding mechanisms. They also impose strict requirements on the mass of the protected object, which has limited their widespread application. Additionally, damping can suppress the system's resonance peak but may weaken the high-frequency isolation effectiveness. In broad-band excitation scenarios, resonance is often unavoidable. Therefore, the vibration system should also have appropriate damping, and additional dampers may be added if necessary.

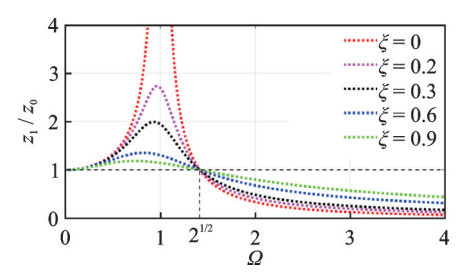


Fig.2 Vibration responses of SDOF systems

#### 1. 2 Flexibility-maximizing structures

Ref.[28] proposed a 2D structural topology optimization algorithm with the goal of minimizing flexibility using the optimization criterion method. For vibration systems, the design objective is to achieve maximum flexibility. Due to non-convexity, it is challenging to obtain suitable results using topology optimization algorithms. Therefore, this study adopts an exhaustive search approach to compare

the flexibility of different structures and ultimately identifies the configuration with the maximum flexibility. The issue with this approach is the high computational demand, which makes it impractical for larger design domains. This study employs DFS and backtracking algorithms to search for the structure with maximum flexibility. The basic idea, as illustrated in Fig.3, involves considering the cell where the load is applied as the starting point and the fixed end as the endpoint. Each path between the starting point and the midpoint is regarded as a potential structure. The finite element method is then used to calculate the flexibility of each structure. Structural flexibility can be expressed as

$$c(x) = U^{\mathsf{T}} K U = \sum_{e=1}^{N} x_e \boldsymbol{u}_e^{\mathsf{T}} \boldsymbol{k}_0 \boldsymbol{u}_e$$
 (6)

where K is the global stiffness matrix of the structure,  $k_0$  the element stiffness matrix, and  $x_e$  the density of the element. To avoid singular solutions, the element densities along the path are set to 1, while the others are set to 0.001.  $u_e$  is the displacement vector and  $k_e$  the element stiffness matrix.

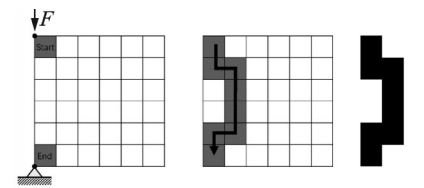


Fig.3 Basic idea of brute-force traversal algorithm

The traversal process is illustrated in Fig.4. Initially, a queue is introduced, where the elements of the queue are stacks, and the elements of the stacks are all possible coordinate points for the next step. The process starts from the starting point and then progresses by selecting a point from the corresponding stack. When the target point is reached, the corresponding path is first output. After that, the target point is deleted and a new point is selected. This process of reselecting paths is called backtracking. The traversal is complete when the queue is empty.

Fig.5(a) shows the calculation results for the maximum flexibility, with the dimensions of the design domain also annotated. It can be observed that the L-shaped folded beam has relatively low stiffness. Based on the results of the traversal search, the

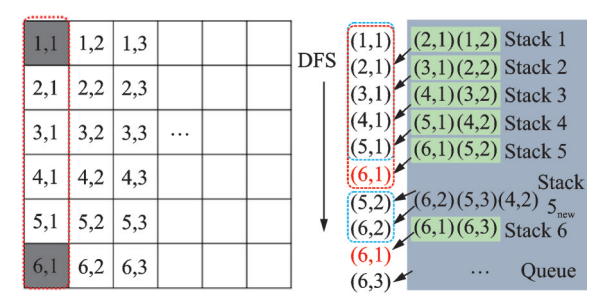
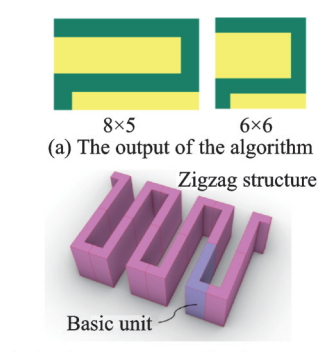


Fig.4 Execution process of algorithm

geometric structure of the vibration isolator has been proposed, as shown in Fig.5(b). This structure, known as the zigzag structure, has also seen some application in the field of vibration isolation<sup>[29-30]</sup>. The calculations in this paper confirm the validity of using the zigzag structure to achieve significant deformation. The basic unit of the zigzag structure is the L-shaped beam, which also determines the final mechanical performance of the isolator.



(b) The basic components of a zigzag structure

Fig.5 Calculation result of zigzag structure

$$\begin{bmatrix} D_{X} \\ D_{Y} \\ D_{Z} \\ \theta_{X} \\ \theta_{Y} \\ \theta_{Z} \end{bmatrix} = \begin{bmatrix} \frac{L}{EA} & 0 & 0 \\ 0 & \frac{L^{3}}{3EI_{Z}} & 0 \\ 0 & 0 & \frac{L^{3}}{3EI_{Y}} \\ 0 & 0 & 0 \\ 0 & 0 & -\frac{L^{2}}{2EI_{Y}} \\ 0 & \frac{L^{2}}{2EI_{Z}} & 0 \end{bmatrix}$$

where  $D_i$  and  $\theta_i$  (i=Z,Y,Z) represent the displacements and rotations at end B in the corresponding directions, and  $F_i$  and  $M_i$  (i=X,Y,Z) the loads applied at the free end of the cantilever beam and the bending moments acting at the free end of the canti-

### 2 Stiffness Calculation of Zigzag Structure

# 2. 1 Deformation calculation of the cantilever

The zigzag structure is composed of beams with constant cross-sections, with the basic unit being the L-shaped beam. The basic unit can be considered as a combination of two cantilever beams. To calculate the stiffness of the structure, the stiffness of the cantilever beam must first be calculated. Fig. 6 shows a 3D cantilever beam AB with a length of L, where end A is fixed and end B is subjected to the force and moment, denoted as F and M, respectively.

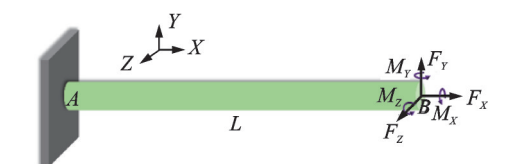


Fig.6 Loading conditions of a 3D cantilever beam

Under the assumptions of linear elasticity and small deformations, the displacement and rotation at end B can be calculated for a single load application. Using the principle of superposition, the overall displacement can be determined. The displacement at end B is expressed as

lever beam. The corresponding directions X, Y, and Z are illustrated in Fig.6.  $I_Y$  and  $I_Z$  the moments of inertia relative to the Y and Z axes. E is the Young's modulus, G the shear modulus, A the cross-sectional area of the cantilever beam, and  $I_P$ 

the polar moment of inertia. For the 2D case shown in Fig.7, it can be simplified to

$$\begin{bmatrix}
 u_{P} \\
 v_{P} \\
 \theta_{P}
\end{bmatrix} = \begin{bmatrix}
 \frac{L}{EA} & 0 & 0 \\
 0 & \frac{L^{3}}{3EI} & -\frac{L^{2}}{2EI} \\
 0 & -\frac{L^{2}}{2EI} & \frac{L}{EI}
\end{bmatrix}
\begin{bmatrix}
 F_{N} \\
 F_{S} \\
 M
\end{bmatrix}$$
(8)
$$\begin{bmatrix}
 EA_{1} \\
 -\frac{F_{X}l_{1}^{3}}{3EI_{1}} - \frac{l_{1}^{2}(M_{C} - F_{Y}l_{2})}{2EI_{1}} \\
 \frac{F_{X}l_{1}^{2}}{2EI_{1}} + \frac{l_{1}(M_{C} - F_{Y}l_{2})}{EI_{1}}
\end{bmatrix}$$
where  $A_{1}$  is the cross-sectional

where  $F_s$  represents the tangential load at the free end,  $F_N$  the circumferential load at the free end, and M the bending moment.



Fig.7 Loading conditions of a 2D cantilever beam

#### **Deformation** calculation L-shaped beam

As shown in Fig.8, the L-shaped cantilever beam ABC is a basic unit of the zigzag structure. It is considered to be a combination of Part 1 and Part 2. The cross-sectional dimensions of the two segments are identical, with lengths denoted as  $l_1$  and  $l_2$ , respectively. The deformation of the L-shaped beam can be calculated by superimposing the deformations of the two cantilever beams.

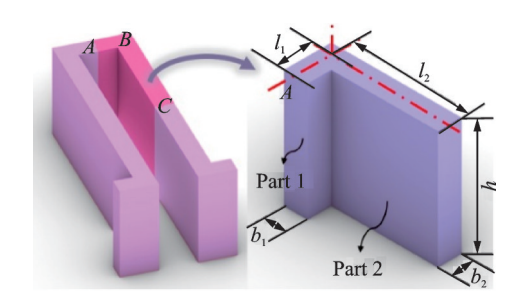


Fig.8 Dimensional parameters of an L-shaped beam

For the cantilever beam AB, the displacement at end B can be expressed as

$$\begin{bmatrix} u_{B} \\ v_{B} \\ \theta_{B} \end{bmatrix} = \begin{bmatrix} \frac{l_{1}}{EA_{1}} & 0 & 0 \\ 0 & \frac{l_{1}^{3}}{3EI_{1}} & -\frac{l_{1}^{2}}{2EI_{1}} \\ 0 & -\frac{l_{1}^{2}}{2EI_{1}} & \frac{l_{1}}{EI_{1}} \end{bmatrix} \begin{bmatrix} F_{Y} \\ -F_{X} \\ M_{C} - F_{Y} l_{2} \end{bmatrix} =$$

$$\begin{bmatrix} \frac{F_{Y}l_{1}}{EA_{1}} \\ -\frac{F_{X}l_{1}^{3}}{3EI_{1}} - \frac{l_{1}^{2}(M_{C} - F_{Y}l_{2})}{2EI_{1}} \\ \frac{F_{X}l_{1}^{2}}{2EI_{1}} + \frac{l_{1}(M_{C} - F_{Y}l_{2})}{EI_{1}} \end{bmatrix}$$
(9)

where  $A_1$  is the cross-sectional area of cantilever beam AB,  $I_1$  the cross-sectional moment of inertia of beam AB, and  $M_C$  the bending moment applied at point C of the L-shaped beam ABC.

At this point, the displacement at end C caused by the deformation at end B can be expressed as

$$\begin{bmatrix} u_{C1} \\ v_{C1} \\ \theta_{C1} \end{bmatrix} = \begin{bmatrix} u_B \\ v_B \\ \theta_B \end{bmatrix} + \begin{bmatrix} -l_2(1 - \cos\theta_B) \\ -l_2\sin\theta_B \\ 0 \end{bmatrix} = \begin{bmatrix} \frac{F_Y l_1}{EA_1} - l_2(1 - \cos\theta_B) \\ -\frac{F_X l_1^3}{3EI_1} - \frac{l_1^2(M_C - F_Y l_2)}{2EI_1} - l_2\sin\theta_B \end{bmatrix}$$
(10)
$$\frac{F_X l_1^2}{2EI_1} + \frac{l_1(M_C - F_Y l_2)}{EI_1}$$

The deformation at end C caused by the applied load can be expressed as

$$\begin{bmatrix} u_{C2} \\ v_{C2} \\ \theta_{C2} \end{bmatrix} = \begin{bmatrix} \frac{l_2}{EA_2} & 0 & 0 \\ 0 & \frac{l_2^3}{3EI_2} & -\frac{l_2^2}{2EI_2} \\ 0 & -\frac{l_2^2}{2EI_2} & \frac{l_2}{EI_2} \end{bmatrix} \cdot \begin{bmatrix} \cos\theta_B & -\sin\theta_B & 0 \\ \sin\theta_B & \cos\theta_B & 0 \\ 0 & 0 & 1 \end{bmatrix} \begin{bmatrix} F_X \\ F_Y \\ M_C \end{bmatrix} = \begin{bmatrix} \frac{l_2}{EA_2} (F_X \cos\theta_B - F_Y \sin\theta_B) \\ \frac{l_2^3}{3EI_2} (F_X \sin\theta_B + F_Y \cos\theta_B) - \frac{l_2^2}{2EI_2} M_C \\ -\frac{l_2^2}{2EI_2} (F_X \sin\theta_B + F_Y \cos\theta_B) - \frac{l_2}{EI_2} M_C \end{bmatrix}$$
(11)

where  $A_2$  is the cross-sectional area of cantilever beam BC, and  $I_2$  the cross-sectional moment of inertia of beam BC.

Thus, the displacement at the free end can be determined as

$$\begin{bmatrix} u_{C} \\ v_{C} \\ \theta_{C} \end{bmatrix} = \begin{bmatrix} u_{C1} \\ v_{C1} \\ \theta_{C1} \end{bmatrix} + \begin{bmatrix} u_{C2} \\ v_{C2} \\ \theta_{C2} \end{bmatrix} = \begin{bmatrix} \frac{l_{2}}{EA_{2}} (F_{X}\cos\theta_{B} - F_{Y}\sin\theta_{B}) + \frac{F_{Y}l_{1}}{EA_{1}} - l_{2}(1 - \cos\theta_{B}) \\ \frac{l_{2}^{3}}{3EI_{2}} (F_{X}\sin\theta_{B} + F_{Y}\cos\theta_{B}) - \frac{l_{2}^{2}}{2EI_{2}} M_{C} - \frac{F_{X}l_{1}^{3}}{3EI_{1}} - \frac{l_{1}^{2}(M_{C} - F_{Y}l_{2})}{2EI_{1}} - l_{2}\sin\theta_{B} \\ - \frac{l_{2}^{2}}{2EI_{2}} (F_{X}\sin\theta_{B} + F_{Y}\cos\theta_{B}) - \frac{l_{2}}{EI_{2}} M_{C} + \frac{F_{X}l_{1}^{2}}{2EI_{1}} + \frac{l_{1}(M_{C} - F_{Y}l_{2})}{EI_{1}} \end{bmatrix}$$

$$(12)$$

#### 2. 3 Stiffness of the zigzag structure

Eq.(11) calculates the displacement at the free end of the L-shaped beam under the action of a load at the free end, allowing us to determine the stiffness of the L-shaped beam. The zigzag structure can be viewed as a linear combination of L-shaped beams. According to the principle of superposition, the stiffness of the zigzag structure can be expressed as

$$K_T = \frac{K_e}{n} \tag{13}$$

where  $K_T$  is the stiffness of the zigzag structure,  $K_e$  the stiffness of the L-shaped beam, and n the number of basic units in series that form the zigzag structure.

## 3 Quasi-static Compression of Zigzag Structure

To verify, a zigzag vibration isolator pad is designed and manufactured. The structure of the isolator is shown in Fig.9. The material of the isolator is TC4, and the elastic modulus of TC4 is 115 GPa.



Fig.9 Schematic diagram of vibration isolator

The isolator employs a symmetric zigzag structure to ensure stable load distribution. Each zigzag structure can be viewed as being composed of 8 sets of L-shaped beams. The thickness of each L-shaped beam is 2 mm, and the width is 30 mm. The length of Part 1 is 3 mm and the length of Part 2 is 6 mm. The stiffness of the isolator pad can thus be calculated as

$$K_T = 2K_e/n = K_e/4$$
 (14)

Using Eq.(11), the compressive stiffness of

the isolator pad is calculated to be approximately 2 778 N/mm. To verify, both simulations and compression experiments are conducted. The simulations are performed using the static general module of Abaqus. The Poisson's ratio for TC4 is set to 0.34, and the Johnson-Cook constitutive model is used with the parameters A=875 MPa, B=793 MPa, and n=0.386.

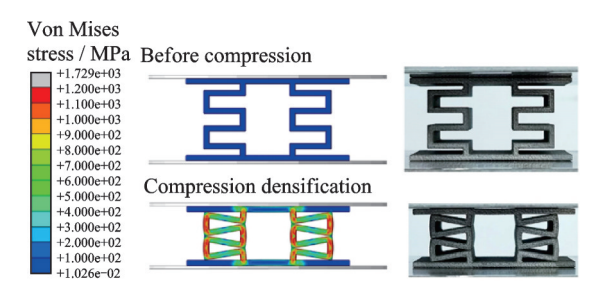


Fig.10 Simulation analysis results of the vibration isolator

The quasi-static compression experiments are conducted on a compression testing machine with a compression rate of 1 mm/min. A comparison of the results from calculations, simulations, and experiments is shown in Fig.11. The results indicate that the calculation method used in this study accurately determines the stiffness of the isolator in the elastic state, with an error of lower than 10% compared to the simulation and experimental results.

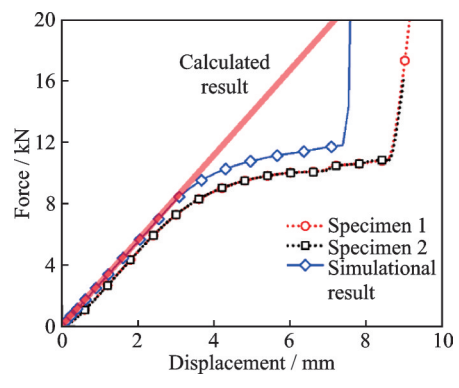


Fig.11 Verification results of the compressive mechanical performance of the vibration isolator

# 4 Applications of Zigzag Vibration Isolator

A certain type of equipment is subjected to random vibration excitation as shown in Table 1, with a root mean square acceleration of approximately 27g. The mass of the protected object is about 0.3 kg, and the vibration reduction efficiency must exceed 50%. The isolator is required to have a length of less than 150 mm, a width of less than 160 mm, and a height of less than 10 mm. Additionally, the isolator must meet certain heat dissipation requirements, so it is specified to be made from a copper-tin alloy using additive manufacturing. The material has an elastic modulus of approximately 110 MPa.

Table 1 Parameters of the random vibration

Parameter	f/Hz				
	20	80	200	300	2 000
Gradient/	+3	_	_	_	_
$(dB \bullet oct^{-1})$					
Power spectral		0.16	0.16	0.40	0.40
density/ $(g^2 \cdot Hz^{-1})$					

When addressing practical issues, a desired natural frequency  $f_n$  is first established. Then, using the formula for calculating natural frequency, the required stiffness of the vibration isolator can be determined.

$$K_{T} = m \left( 2\pi f_{p} \right)^{2} \tag{15}$$

For example, in this case, if the desired natural frequency is  $f_{\rm n} = 120$  Hz, the required stiffness of the vibration isolator is approximately 170 N/mm. By adjusting the dimensions and number of L-shaped beams, the stiffness of the isolator can be made to approach the desired value.

The design and physical prototype of the isolator are shown in Fig.12. This vibration isolator consists of four parallel zigzag structures, with each zigzag structure composed of 8 L-shaped beams. The dimensions of each L-shaped beam are as follows: the length of the vertical beam is 1 mm, the horizontal beam is 16 mm, the beam thickness is 1 mm, and the overall length is 50 mm.

As a result, the overall stiffness of the isolator



Fig.12 Geometric structure of vibration isolator

is calculated to be approximately 140 N/mm, corresponding to a natural frequency of about 108 Hz. Vibration experiments are conducted as per the testing plan shown in Fig.13. The vibration bench used is the SUSHI Company's DC Test Stand, and two acceleration sensors are installed on the protected object.

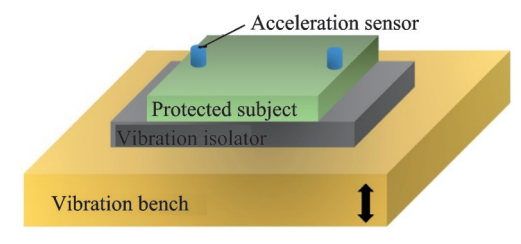


Fig.13 Schematic diagram of vibration experiments

The results of the sweep frequency test for the vibration system, ranging from 20 Hz to 2 000 Hz, are shown in Fig.14. The acceleration during the sweep was 1g. From the figure, it can be observed that the first-order resonance frequency of the vibration system is approximately 90 Hz. This indicates that the zigzag vibration isolator is effective in lowering the first-order resonance frequency of the vibration system. The random response of the vibration under specified excitation is shown in Fig.15. The results from the figure indicate that the vibration isolator effectively reduces vibrations, with a vibration reduction efficiency exceeding 60%.

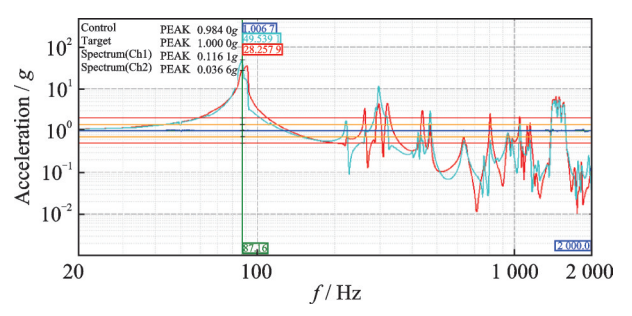


Fig.14 Sweep frequency test results

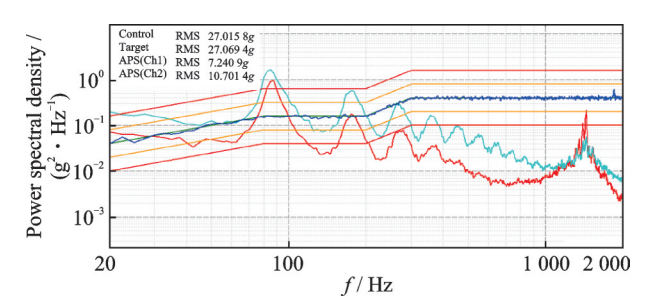


Fig.15 Random vibration test results

#### 5 Conclusions

Based on additive manufacturing processes, this paper proposes a new type of vibration isolator configuration. The harmonic response analysis of SDOF system indicates that, under broad frequency excitation conditions, a high-flexibility isolator can achieve a wider vibration reduction bandwidth. Using traversal algorithms, the structure with high flexibility in a 2D scenario is calculated, and it is shown that the L-shaped cantilever beam configuration provides the maximum flexibility. Based on this, the structural stiffness of the zigzag isolator is calculated, and quasi-static compression experiments demonstrate that the theoretical calculations and experimental results have an error of lower than 10%. Finally, the zigzag isolator is applied to a practical engineering scenario, and the results show that the zigzag isolator can effectively reduce the first-order resonance frequency of the vibration system, with a vibration reduction efficiency exceeding 60% under given random vibration excitation.

#### References

- [1] LUY, LIUJ, YANGH, et al. Research on automatic test system of engine blade natural frequency[J].

  Transactions of Nanjing University of Aeronautics and Astronautics, 2024, 41(4): 476-487.
- [2] JIA M, DAI N, GE Y, et al. Design of an ultrathin passive isolator based on multi-layer plain-woven wire mesh[J]. Mechanical Systems and Signal Processing, 2024, 208: 110988.
- [3] LOU J, SUN J, TANG S, et al. Study on the optimization of the shock isolation system based on the limiting performance analysis[J]. International Journal of Dynamics and Control, 2014, 2(3): 415-424.

- [4] NOWAK A, CAMPANILE L F, HASSE A. Vibration reduction by stiffness modulation—A theoretical study[J]. Journal of Sound and Vibration, 2021, 501: 116040.
- [5] HO C, LANG Z Q, BILLINGS S A. Design of vibration isolators by exploiting the beneficial effects of stiffness and damping nonlinearities[J]. Journal of Sound and Vibration, 2014, 333(12): 2489-2504.
- [6] IBRAHIM R A. Recent advances in nonlinear passive vibration isolators[J]. Journal of Sound and Vibration, 2008, 314(3/4/5): 371-452.
- [7] SUN W, THOMPSON D J, ZHOU J, et al. Analysis of dynamic stiffness effect of primary suspension helical springs on railway vehicle vibration[J]. Journal of Physics, 2016, 744(1): 012149.
- [8] BHATT C D, NADARAJAN M, BALAJI R, et al. Leaf spring model for heavy load vehicle using solid works and ANSYS analysis[J]. Materials Today: Proceedings, 2020, 33: 4764-4770.
- [9] DONGHUI L I, ZHENWEI F, JIAN Z, et al. Optimum design and experiment of composite leaf spring landing gear for electric aircraft[J]. Chinese Journal of Aeronautics, 2020, 33(10): 2649-2659.
- [10] KANG K J. Wire-woven cellular metals: The present and future[J]. Progress in Materials Science, 2015, 69: 213-307.
- [11] REN Z, SHEN L, BAI H, et al. Constitutive model of disordered grid interpenetrating structure of flexible microporous metal rubber[J]. Mechanical Systems and Signal Processing, 2021, 154: 107567.
- [12] YANG P, BAIH, XUE X, et al. Vibration reliability characterization and damping capability of annular periodic metal rubber in the non-molding direction[J]. Mechanical Systems and Signal Processing, 2019, 132: 622-639.
- [13] RASHIDI S, ZIAEI-RAD S. Experimental and numerical vibration analysis of wire rope isolators under quasi-static and dynamic loadings[J]. Engineering Structures, 2017, 148: 328-339.
- [14] TINKER M L, CUTCHINS M A. Damping phenomena in a wire rope vibration isolation system[J]. Journal of Sound and Vibration, 1992, 157(1): 7-18.
- [15] YANG Y, SHAN M, ZHAO L, et al. Multiple strut-deformation patterns based analytical elastic modulus of sandwich BCC lattices[J]. Materials & Design, 2019, 181: 107916.
- [16] ALAÑA M, LOPEZ-ARANCIBIA A, PRADERA-

- MALLABIABARRENA A, et al. Analytical model of the elastic behavior of a modified face-centered cubic lattice structure[J]. Journal of the Mechanical Behavior of Biomedical Materials, 2019, 98: 357-368.
- [17] HULL, CAIDY, WUGP, et al. Influence of internal pressure on the out-of-plane dynamic behavior of circular-celled honeycombs[J]. International Journal of Impact Engineering, 2017, 104: 64-74.
- [18] CLARKE D J, IMEDIEGWU C, MOAT R, et al.
  A systematic numerical and experimental study into
  the mechanical properties of five honeycombs[J].
  Composites Part B: Engineering, 2023, 264: 110895.
- [19] JIA M, DAI N, WANG T, et al. A compact quasizero stiffness metamaterial for energy absorption and impact protection[J]. Thin-Walled Structures, 2024, 205: 112360.
- [20] ZHANG L, FEIH S, DAYNES S, et al. Energy absorption characteristics of metallic triply periodic minimal surface sheet structures under compressive loading[J]. Additive Manufacturing, 2018, 23: 505-515.
- [21] FENG G, LI S, XIAO L, et al. Mechanical properties and deformation behavior of functionally graded TPMS structures under static and dynamic loading[J]. International Journal of Impact Engineering, 2023, 176: 104554.
- [22] SANTIAGO R, RAMOS H, ALMAHRI S, et al. Modelling and optimisation of TPMS-based lattices subjected to high strain-rate impact loadings[J]. International Journal of Impact Engineering, 2023, 177: 104592.
- [23] CHEN Y, QIAN F, ZUO L, et al. Broadband and multiband vibration mitigation in lattice metamaterials with sinusoidally-shaped ligaments[J]. Extreme Mechanics Letters, 2017, 17: 24-32.
- [24] HANS, PHAMTM, TRANTT, et al. Mechanical properties and energy absorption of bio-inspired hierarchical circular honeycomb[J]. Composites Part B: Engineering, 2022, 236: 109818.
- [25] XU J, CHANG L, CHEN T, et al. Study of the bending properties of variable stiffness chain mail fabrics[J]. Composite Structures, 2023, 322: 117369.
- [26] ZHANG Q, GUO D, HU G. Tailored mechanical metamaterials with programmable quasi-zero-stiffness features for full-band vibration isolation[J]. Advanced Functional Materials, 2021, 31(33): 2101428.

- [27] CAIC, ZHOU J, WU L, et al. Design and numerical validation of quasi-zero-stiffness metamaterials for very low-frequency band gaps[J]. Composite Structures, 2020, 236: 111862.
- [28] SIGMUND O. A 99 line topology optimization code written in Matlab[J]. Structural and Multidisciplinary Optimization, 2001, 21(2): 120-127.
- [29] ZHANG J, ZHANG X, ZHANG H, et al. Rainbow zigzag metamaterial beams as broadband vibration isolators for beam-like structures[J]. Journal of Sound and Vibration, 2022, 530: 116945.
- [30] ABDELJABER O, AVCI O, KIRANYAZ S, et al. Optimization of linear zigzag insert metastructures for low-frequency vibration attenuation using genetic algorithms[J]. Mechanical Systems and Signal Processing, 2017, 84: 625-641.

**Acknowledgements** This work was supported by the National Key Research and Development Program of China (Nos. 2023YFB4603900, 2023YFB4603901) and the National Natural Science Foundation of China (No.52275255).

#### Authors

The first author Dr. JIA Meng is currently a postdoctoral researcher at Nanjing University of Aeronautics and Astronautics. His research focuses on the design of lightweight vibration-damping functional structures.

The corresponding author Prof. DAI Ning received the B.E., M.S., and Ph.D. degrees from Nanjing University of Aeronautics and Astronautics. Now he is a professor at Nanjing University of Aeronautics and Astronautics, primarily engaged in research and development in intelligent digital design, bionic design and manufacturing, additive manufacturing technology.

Author contributions Dr. JIA Meng conducted the literature review, performed the technical analysis, and drafted the initial manuscript. Mr. WANG Tingwei designed the study, contributed to the development of the methodology, and critically revised the manuscript. Prof. DAI Ning provided technical guidance on modeling strategies, supervised the project, and advised on the research topic. All authors commented on the manuscript draft and approved the submission.

**Competing interests** The authors declare no competing interests

### 一种基于增材制造的紧凑型锯齿隔振器

贾 梦,王莲葳,戴 宁

(南京航空航天大学机电学院,南京 210016,中国)

摘要:复杂环境激励通常会对飞行器设备的运行安全构成威胁。由于无需额外能源供应的优势,被动隔振技术得到了广泛应用。本文提出了一种基于锯齿结构的新型金属隔振器,结构紧凑并可通过增材加工制备,易于实现结构-功能的一体化。首先,建立单自由度(Single-degree-of-freedom, SDOF)振动系统的控制方程并分析其频响特性,结果表明有效隔振的前提是隔振器具备足够低的刚度。为获得低刚度、高柔顺度结构,文中结合回溯遍历算法与有限元方法(Finite element method, FEM)对结构进行优化设计后得到锯齿结构构型。随后,建立锯齿结构的参数化几何模型并分析其几何-刚度的映射关系,然后进行准静态压缩试验验证。最后,针对某工程应用场景的实际需要设计并制备锯齿隔振器。振动试验结果表明,所设计的锯齿隔振器能有效降低系统刚度与基频,减振效率超过60%。

关键词:振动隔离;被动减振;增材制造;锯齿结构;金属隔振器